

Numerical assessment of influence of confining stress on Kaiser effect using distinct element method

M. Nikkhah

School of Mining, Petroleum & Geophysics Engineering, Shahrood University of Technology, Shahrood, Iran

Received 11 December 2015; received in revised form 26 July 2016; accepted 9 September 2016
Corresponding author: m.nikkhah@shahroodut.ac.ir (M. Nikkhah).

Abstract

Nowadays acoustic emission (AE) testing based on the Kaiser Effect (KE) is increasingly used to estimate the in-situ stress in laboratories. In this work, this effect is assessed on cylindrical specimens in numerical simulations of the cyclic loadings including loading, unloading, and re-loading cycles using a 3D code called the particle flow code (PFC) based upon the distinct element method. To achieve this objective, at first, the numerical model is calibrated using a laboratory test performed on the selected sandstone specimens. The results obtained show that PFC and the distinct element code are useful tools used to investigate the damage and KE of a brittle rock. Also the results obtained by the triaxial modeling show that a combination of triaxial loading stresses change the results of uniaxial loading. Further, KE is influenced under confining stresses so that larger confining stresses lead to greater differences between the KE stress during the uniaxial and pre-stress loadings.

Keywords: *Kaiser Effect, Confining Stress, Numerical Modeling, Rock, Particle Flow Code.*

1. Introduction

The in-situ stress in a rock mass is a key parameter of the rock engineering projects in civil, mining, and petroleum engineering. There are various methods implemented to predict the in-situ stress, the most common of which is the hydraulic fracturing (HF) method, which is both expensive and time-consuming. As a matter of fact, these days, laboratory methods based on drilled "core" have gained popularity, considering their simple, cheap, and quick applications. In this regards, several methods have been proposed to estimate the in-situ stresses from cored rock samples. One such method that can be carried out in the laboratory conditions is the acoustic emission (AE) technique that utilizes the Kaiser Effect (KE) phenomenon.

Generally, rocks and most materials emit sounds and seismic signals with high frequencies, which are called AE. This is caused as a result of the micro-crack closure of the propagation, dislocations, grain boundary movement, and fracture propagation in or between grain

boundaries, crack formation in grain structure, and shear fracture. It is believed that there should be a significant relationship between a rock damage and AE. The Kaiser Effect (KE) was named after J. Kaiser, whose pioneering research work allowed concluding the possibility of determining previous stresses [1, 2]. KE is defined as the absence of detectable AE until previously-applied stress levels are exceeded. In this regard, AE is investigated for the cyclic loading in a stress path on the rock specimens. In other words, during the first loading cycle, the AE activity is observed at all stress levels but, in the next reloading cycles, AE is not seen or is decreased at stress levels lower than the previous maximum stress. When the stress applied to the second cycle exceeds the previous maximum stress, there is a sudden increase in the AE activity with the corresponding stress being considered as the KE stress point (Figure 1). AE is monitored by acoustic sensors, which are often of piezoelectric type in a laboratory environment.

The KE method is based upon the assumption that under repeated loads, a rock will not generate new cracks or extend the pre-existing cracks when the stress is lower than the previous maximum stress. Therefore, the source of AE under compression is believed to be the crack generation/growth. Some researchers refer to this mechanism as the damage accumulation.

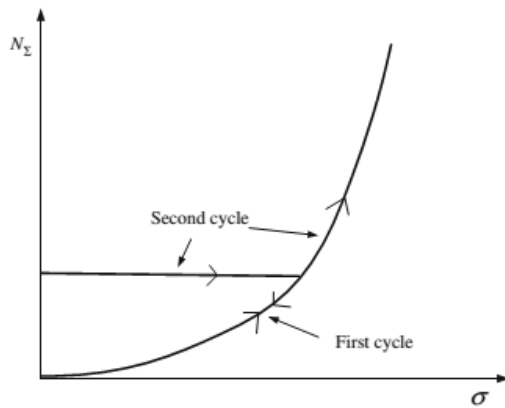


Figure 1. Cumulative AE hits (N_{Σ}) versus stress (σ) in two successive cycles of uniaxial compression [2].

In most engineering projects, an anticipation of possible complication conditions and their different states is essential. Nowadays the anticipation and design of most plans can be carried out by numerical methods so that they can be simulated by computer models under identical conditions similar to reality in order to obtain a logical consequence and replication.

The KE simulation can be developed using the principles of continuum damage mechanics (CDM). This has been shown by Tang and Kou (1998), who developed a model based on the damage theory and the AE under cyclic uniaxial stress of rocks [3]. Chen et al. (2007) have investigated numerical and experimental studies on the directional dependence of KE in granite. In their studies, KE of rocks was simulated by a numerical simulation method using the rock failure process analysis (RFPA2D) software on cubic rock specimens under two perpendicular loading conditions [4]. Lavrov et al. (2002) have studied KE in the cyclic Brazilian test by rotating the disk specimen during the cyclic loadings. Their studies were based upon the 2D boundary element method and the discontinuity interaction and growth simulation (DIGS) code, as applied to the numerical simulation, and the influence of the first loading on the subsequent loading in the orthogonal direction was examined. Their results showed that when the rotation angle in the second cycle of loading was greater than 10 degrees, KE

did not appear [5, 6]. Hunt et al. (2003) have used PFC 2D for the numerical simulation of KE [7]. Holt et al. (2005) and Gorodkov et al. (2006) have studied the simulation effect of releasing the stress of rock coring from the deep borehole, and used the rock stress memory to determine the previously-experienced stress level using the PFC software. They concluded that the KE could be applied to the horizontal in-situ stress measurement [8, 9]. The main purpose of the DEM modeling conducted in this study was to supplement the previous research works conducted regarding the numerical modeling of KE of a rock. Although the use of the KE to determine the in-situ stress has still remained controversial, there are a number of studies where it has been successfully applied. The particle flow code (PFC) software was employed in this work since it allowed implementing the discrete element analysis. It is increasingly used in geotechnical engineering applications to model the non-homogeneous and discontinuous materials. The objective of this work was to investigate a numerical model based on the 3D DEM to simulate KE, and to evaluate the influence of confining stress on it.

2. 3D particle flow code (PFC 3D)

PFC is a distinct element modeling program, in which a rock is represented by an assembly of particles bonded together at contact points [10]. This code enables the simulation of fracture initiation and propagation, thereby, providing the possibility of tracking the number and position of the cracks. In the bonded particle model (BPM), as opposed to the indirect fracture simulation, the damage is represented directly by the formation of cracks [11]. Each particle in the PFC model is assigned a normal and shear stiffness. The particles are rigid, and the contacts are allowed in a very small area between particles. Two types of bonds are typically used in PFC: the contact bond and the parallel bond. In the contact bond model, an elastic spring with constant normal and shear stiffnesses, K_n and K_s , acts at the contact points between particles, thus allowing only forces to be transmitted. In the parallel bond model, the moment induced by particle rotation is resisted by a set of elastic springs uniformly distributed over a finite-sized section lying on the contact plane and centered at the contact point. This bond model reproduces the physical behavior of a cement-like substance gluing adjacent particles together [10, 12]. Therefore, in this work, the parallel bond model was used to simulate the behavior of the

cemented sandstone rock. Figure 2 shows the principle and the force-displacement relationship for the parallel bond model. There is a certain area and stiffness bonding in the contact points of the parallel bond model, which can limit the particles' rotation and transmit force and torque. Under loading, the stresses in parallel bond can be obtained via the beam theory through the following formula (1):

$$\bar{\sigma} = \frac{-\bar{F}_i^n}{A_2} + \frac{|\bar{M}_i^s| \bar{R}}{I}$$

$$\bar{\tau} = \frac{-\bar{F}_i^s}{A_2} + \frac{|\bar{M}_i^n| \bar{R}}{J}$$
(1)

where \bar{F}_i^n , \bar{F}_i^s ; \bar{M}_i^n , and \bar{M}_i^s are the force components and moments about the center of the cemented contact zone, and A, I, and J denote the area, polar moment of inertia of the disk, and moment of inertia of the bond disk, respectively, and in ($A = \pi \bar{R}^2$; $J = \pi \bar{R}^4/2$; $I = \pi \bar{R}^4/4$), \bar{R} is the average radius for the parallel bond contact in the contact point. When the normal stress exceeded $\bar{\sigma}$ or the tangential stress exceeded $\bar{\tau}$, the parallel bond was damaged, respectively, generating tension micro-cracks or shear micro-cracks [10, 11].

The bond breakage in PFC represents the formation of cracks (Figure 3). The micro-crack initiation and propagation can be expressed as a progressive breakage of contact bonds [13].

Zhang and Wong (2012) have numerically simulated the cracking process in a rock-like material containing a single flaw under uniaxial compression. The coalescence behavior for the case of two-stepped and co-planar pre-existing open flaws have been investigated by Zhang and Wong (2013) [14, 15].

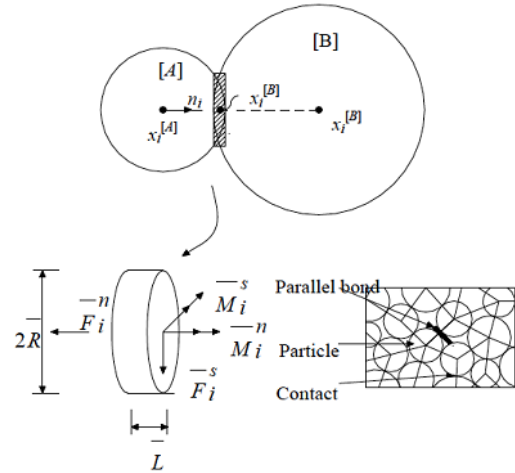


Figure 2. Principle and force-displacement relationship for parallel bond model [10].

Within the last decade, the application of PFC in numerical simulation of the crack propagation, fracturing, and hydraulic fracturing of rocks have been the subject of growing attention by many researchers [8, 16-22].

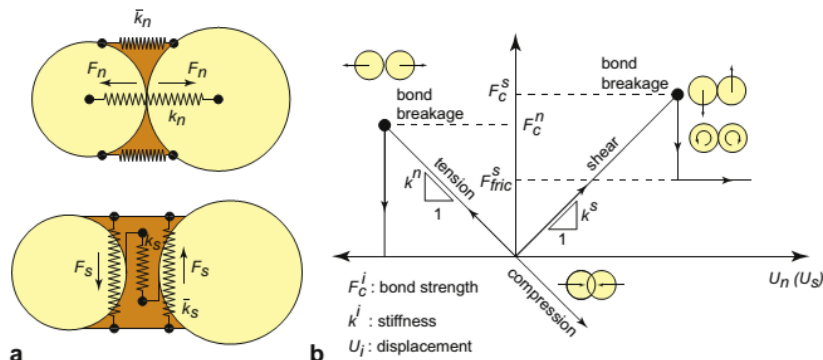


Figure 3. Parallel bond model implemented in PFC. (a) Normal and shear stiffnesses between particles. Contact stiffnesses, k_n and k_s , remain active even after bond breaks as long as particles stay in contact. Bond stiffnesses (per unit area), k_n and k_s , are suddenly removed when bond breaks regardless of whether particles stay in contact. (b) Constitutive behavior in shear and tension [11].

3. Numerical modeling of KE

Since sandstone is a sedimentary rock composed of cemented grains, it can be modeled perfectly by PFC. As stated earlier, since this code is based upon the algorithm of the distinct element method, it is superior to the continuous modeling methods, which justify its adoption in the present research

work. On the other hand, as KE has been raised micro-mechanically by the formation of cracks in rocks, it cannot be easily described in terms of the continuous theories. Therefore, PFC, which utilizes BPM, was used in the present work.

3.1. Sample calibration and determination of input parameters

In PFC modeling, the model calibration is necessary to simulate the macroscopic behavior of a rock so that the set of properties and micro-parameters are selected. In this code, unlike the other ordinary engineering codes, the rock is required to be synthesized. While the selected properties are easily attributed to the PFC model, it is often difficult to select the properties of the model to be represented in a real physical sample.

The macro-scale properties of the synthesized rock are determined through laboratory simulation of the rock sample. These macro-properties are the same as those measured in the laboratory. The calibration of a PFC model requires adjusting the micro-parameters to achieve the strength properties determined in a laboratory test. Generally, the suitable micro-parameters of the model are determined during the calibration, in which the response of the synthetic material is directly compared with that of the real material. There is no advanced theory available to incorporate the transformation of the macro-parameters into the micro-parameters in the modeling. Therefore, a model calibration was performed by means of the trial and error method. In PFC, the solid rock is represented by an assembly of particles contacted together by breakable bonds. The parallel bond rock models have been widely used to study the fracturing and fragmentation processes in brittle rocks. However, one of the major drawbacks of this type of model is the unrealistically low ratios of the simulated unconfined compressive strength to the indirect tensile strength for synthetic rock specimens [23, 24]. The straightforward adoption of circular (or spherical) particles cannot fully capture the behavior of complex-shaped and highly-interlocked grain structures that are typical of hard rocks. Cho et al. (2007) have shown that by applying a clumped-particle geometry, a significant reduction of the aforementioned deficiencies can be obtained, thereby, allowing one to reproduce correct strength ratios, non-linear behavior of strength envelopes, and friction coefficients comparable with laboratory values [11].

A clump of particles behaves like a rigid body but the contacts out of group are not affected and contacts arise when the particles forming the group boundary interact with other particles. The group behavior resembles a rigid body (with deformable boundary) that, regardless of the forces on it, is not broken. In this respect, a clump

is different from a cluster of connected particles [22-23, 25]. One advantage of the cluster model of particles is a more accurate and realistic modeling of the rock grain behavior, complex interactions of grains, and an accurate and realistic formation of cracks in the model. According to the studies of Potyondy and Cundall (2004), there is a difference between the results of ultimate strength and the envelope of numerical and laboratory modeling in high-confining stresses in triaxial tests.

To reduce such differences and achieve a more realistic behavior model, further analyses are required. The cluster of particle model is used to model particles, which can somewhat alleviate the difference. To increase the final stress levels in higher pressures, and partly overcome this problem, the cluster particle model can be used to model the rock, which can partly improve the results and reduce the difference between the maximum strengths of experimental data envelope and numerical data. This method has been used by Martin et al. (2007) in a 2D PFC modeling of Lac Du Bonnet granite, and desirable results have been achieved. It should be noted that for 3D models, more extensive research works are required to model the non-linear behavior in higher confining pressures. Given the superiority of the model clump, its particles were used in the modeling of the current work.

The dimensions of the numerical model samples were selected according to the mechanical tests, relevant mechanical properties of rock, and determination method. The dimensions of the calibration model sample were chosen as a height of 120 mm and a diameter of 54 mm.

The compression tests were performed in a polyaxial cell. The top and bottom walls of the model cell acted as loading platens, and the velocities of the side-walls were controlled by a servo-mechanism to maintain a constant confining stress. The modeling of the uniaxial and fully unconfined tests can be performed by removal of all of the side-walls, which are performed by setting the relevant PFC parameter value equal to a non-zero. All walls were frictionless, and the normal stiffness of the platen walls and the confining walls were set equal to the average particle normal stiffness of the material. The compression test begun with a seating phase, and the axial and confining stresses were applied by activating the servo-mechanism algorithm so that the servo-behavior was controlled by the wall-servo tolerance. The specimen was loaded by moving the platens toward one another at a final velocity, which was determined by specifying the

strain rate. The platen acceleration at the start of loading was controlled by specifying the appropriate values. The platen velocity was adjusted to reach a final value in a sequence of stages.

Using the 85 uniaxial compression models and the trial and error method, the calibrated parameters were selected according to the properties of the stress-strain behaviors of the laboratory and real sandstones, as shown in Table 1. The stress-strain curve of the numerical modeling behavior and experimental model calibration is shown in Figure 4. As it can be seen,

the uniaxial strength and elastic modulus of the numerical model were also compared with the experimental data, and favorable results were achieved. The comparison between the results for the uniaxial strength, Poisson's ratio, Young's modulus, stress-strain curve behavior, and triaxial strength envelop of numerical model, and laboratory tests indicated the accuracy of the calibration and the selection of its appropriate parameters. In Table 2, the macroscopic properties obtained by performing the calibrated model and the physical properties of the sandstone sample are given.

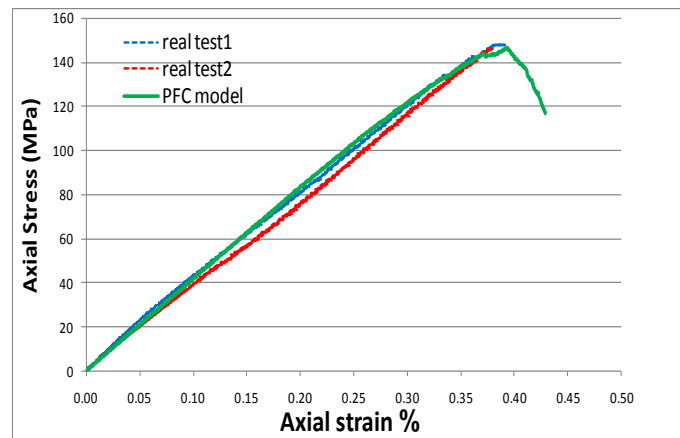


Figure 4. Comparison between stress-strain curves of calibrated numerical model and experimental model under uniaxial testing.

Table 1. Micro-parameters of numerical model.

Micro-Parameter	Value	Micro-Parameter	Value
E (gpa) Young's modulus of particle	34	Density (kg/m ³)	2685
Ratio of minimum radius to maximum radius	1.6	Minimum radius of grains (m)	1.8×10^{-3}
Young's modulus of parallel bond (gpa)	34	Coefficient of friction	0.7
$\bar{\sigma}_c$ (std. dev.) Shear strength of parallel bond, standard deviation (mpa)	52	$\bar{\tau}_c$ (mean) Shear strength Parallel bond, mean (mpa)	155
$\bar{\sigma}_c$ (std. dev.) Normal strength, parallel bond, standard deviation (mpa)	52	$\bar{\sigma}_c$ (mean) Normal strength Parallel bond, mean (mpa)	155
Normal stiffness to shear stiffness of particles $\left(\frac{k_n}{k_s} \right)$	1.2	Ratio of normal stiffness to shear stiffness of parallel bond $\left(\frac{\bar{k}_n}{\bar{k}_s} \right)$	1.2

Table 2. Macro-properties of physical sample and numerical model.

Material	Density (Kg/m ³)	UCS [Mpa]	Young's modulus [Gpa]	Poisson's ratio	Porosity %	P-wave velocity (m/sec)
Real sandstone	2680	143.2	38.7	0.18	0.92	4567
Synthetic sandstone model	2685	144.3	38	0.178	-	-

3.2. Numerical modeling procedure

The numerical modeling procedure of KE similar to what is carried out in the laboratory was implemented. To determine the point of KE, the micro-crack number curves with respect to the stress in the reloading cycle of models were used. The numerical simulation modeling of KE includes the following strategy and steps:

- Creating an initial model and the base sample
- Calibrating the model and selecting the micro-parameters
- Applying the loading, unloading, and re-loading cycles
- Determining the KE point

3.3. Numerical model samples

As mentioned earlier, the numerical studies on KE were carried out on the sandstone samples with cylindrical geometry. Thus cylindrical specimens with a height and diameter of 110 and 54 mm, respectively, were loaded axially under uniaxial compression after the confining pre-loading.

3.4. Loading paths of numerical modeling

Cylindrical numerical samples with different confining pressures were used to show the effect of combining confining stress in KE. During the simulations, each bond breakage was assumed to be a micro-crack. Under the uniaxial and triaxial conditions, the following three paths of loading on synthetic cylinder numerical samples were considered:

A) Loading path (I): loading and un-loading in the direction of the axis (σ_1) under uniaxial stress condition and the reloading in the pre-loading direction under uniaxial condition

B) Loading path (II): triaxial loadings (σ_3) and (σ_1) in triaxial stress conditions, unloading, and re-loading in the vertical direction under the uniaxial condition

C) Loading path (III): triaxial loading (σ_3) and (σ_1), unloading and re-loading (σ_3) and (σ_1) under triaxial condition

3.4.1. Loading path (I)

In this research work, the numerical modeling capabilities in re-producing KE in uniaxial compression were studied. In this regard, the maximum pre-stress values in uniaxial models of the cylindrical samples were 20, 25, 35, 65, 85, and 110 MPa. Surprisingly, the maximum stress

values at pre-loading were greater than the threshold of crack onset in the PFC program. It is because by defining the parameter calibration performed in the modeling, cracking at the stress level would be greater than the threshold parameter defined. As a result, since the crack growth is also a source of AE, an examination of stress memory at pre-stress levels less than 8.4 MPa would be impossible. In the numerical model of uniaxial compression tests, the crack onset stress, i.e. σ_{ci} was 8.4 MPa, so if the maximum stress in the preloading becomes smaller than this value, the effect of stress memory will be invisible. If the pre-loading is applied at a stress level greater than σ_{ci} , some cracks will be formed permanently in the sample. In other words, if the pre-loading stress under uniaxial condition is $\sigma_{ci} < \sigma_p$, KE will not appear. Figure 5 shows the plots of the cumulative total number of recorded cracks in terms of axially-loaded stress in pre-loading and loading cycles as well as the re-loading for the pre-stresses of 25 and 65 MPa.

Generally, the graphs derived from numerical simulations closely resemble laboratory tests so that micro-cracks do not emerge before reaching the stress level of the previous preloading in uniaxial conditions, with its onset and propagation being due to damage caused during the re-loading cycle. The breakage of new bonds is due to the excessive level of stress from the threshold of crack onset in the bond. The failure of the bond is confirmed with the monitoring of a number of broken bonds equal to micro-cracks cumulatively. As shown in these figures, in the re-loading cycle, when the stress level exceeds the previous stress level of the pre-loading, the increasing trend of cracks indicates the retrieval of KE. However, in the sample pre-stress of 20 MPa, the onset stress of cracking, i.e. the KE point, is greater than the pre-stress applied to the samples. These values for the pre-stress of 20 MPa give a retrieved stress value of 21 MPa. Thus the felicity ratio at this stress level is greater than one, and for other stress levels, the stress retrieved from the re-loading is equal to the pre-loading stress with a felicity ratio of one. (Felicity ratio is the ratio of the amount of stress in which the increasing AE reaches the maximum stress of the previous loading).

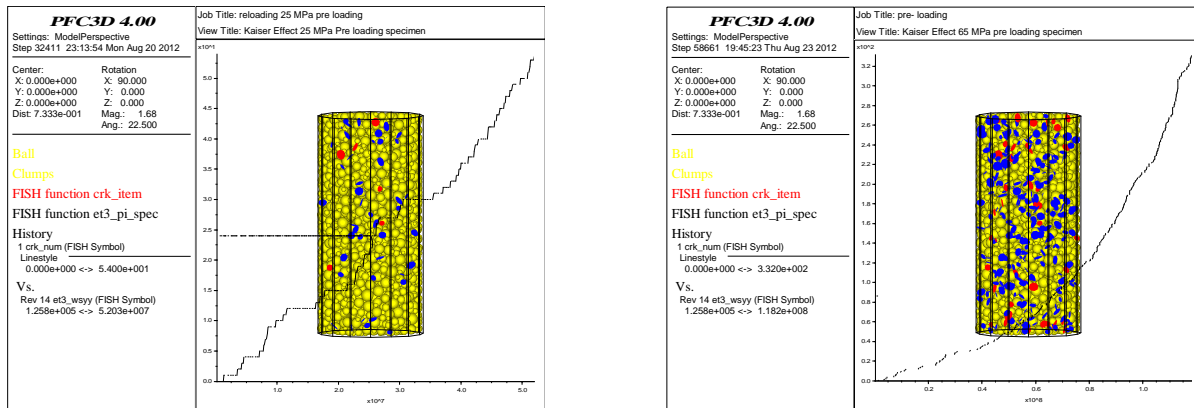


Figure 5. Cumulative total number of recorded cracks versus loading stress under uniaxial modelling in axial preloading for pre-stresses of 25 MPa (left) and 65 MPa (right).

3.4.2. Loading path (II)

The triaxial simulations of KE in this loading path were performed in the way that the models were loaded in a triaxial stress at different levels of confining, and axial stresses and reloading were carried out after the pre-loading of the confining and axial stresses of specimen or under the uniaxial pressure along the perpendicular axis to the stress level greater than the loading stress level. The pre-loading stress combinations were considered to determine the effect of triaxial pressure as well as the stress levels at different

stages of triaxial stress-strain behavior curve of rock. In this loading path, the axial pre-loading at stress levels of 20, 30, 35, 65, 85, and 110 MPa, and at different confining pressures were applied. In Table 3, the results of numerical modeling of cylindrical samples in the loading path II including the KE, the ratio of the KE stress to the axial pre-stress, and the KE stress to the difference between the axial and confining stresses are presented.

Table 3. Results of numerical modeling of cylindrical samples (loading path II).
Triaxial pre-stress (MPa)

Sample	$\frac{\sigma_{KE}}{\sigma_{IP}}$	σ_{3P}	σ_{KE} (Mpa)	K	$\frac{\sigma_{KE}}{\sigma_{IP}}$	$\frac{\sigma_{KE}}{\sigma_{IP} - \sigma_{3P}}$
1	20	5	17	-0.4	0.85	1.1
2	20	10	11	-0.1	0.55	1.1
3	20	15	7	-0.1	0.35	1.4
4	20	30	22	-1.06	1.1	-2.2
5	30	5	22	0.6	0.73	0.8
6	30	10	16	0.4	0.53	0.8
7	35	5	25	1	0.7	0.8
8	35	10	18	0.7	0.5	0.7
9	35	15	17	0.2	0.4	0.8
10	35	20	16	-0.05	0.4	1.06
11	35	50	27.5	-0.8	0.7	-1.8
12	65	15	38.5	1.4	0.4	0.57
13	65	20	37	0.4	0.5	0.82
14	65	30	33	0.06	0.5	0.97
15	65	50	22.5	-0.15	0.3	1.5
16	65	80	33	-0.6	0.5	-2.2
17	85	10	58	1.7	0.6	0.7
18	85	15	50	1.3	0.5	0.7
19	85	20	42	1.15	0.4	0.6
20	85	50	38	-0.06	0.4	1.08
21	85	70	36	-0.3	0.4	2.4
22	85	100	50	-0.65	0.5	-3.3
23	110	10	88	1.2	0.8	0.88
24	110	15	84	0.7	0.7	0.8
25	110	20	65	1.25	0.5	0.7
26	110	50	52	0.16	0.4	0.8
27	110	70	42	-0.02	0.3	1.05
28	110	80	40	-0.1	3.3	1.3
29	110	125	58	-0.5	0.5	-3.8

The coefficients K , $\frac{\sigma_{KE}}{\sigma_{1p}}$, and $\frac{\sigma_{KE}}{\sigma_{1p} - \sigma_{3p}}$, calculated from each model to determine KE in the corresponding model, are presented in the table above. K is a dimensionless coefficient, and characterizes the slope of the damage surface projection on the plane $(\sigma_1 - \sigma_3)$ versus σ_3 . According to the results obtained, as shown in Figure 6, in the cases where $\sigma_{1p} > \sigma_{3p}$, an increased confining pressure can lead to a reduction in the KE stress. During un-loading under high confining pressure, the micro-cracks are observed due to the release of stress, e.g. 50 and 70 MPa confining pressures. Thus when the confining stress is released from the sample, the breakage of bonds is resulted. The stress memory effect is more sensitive to confining stresses compared with the axial loading stress so that greater ratios would lead to higher clarity in identifying and assessing KE. It means that recognition of the KE point is more difficult than the related ratio approach one. As shown in the table, under

$\sigma_{1p} > \sigma_{3p}$, a reduction in the damage coefficient K is associated with the increased confining pressure. The growth and number of micro-cracks in the samples subjected to triaxial loading declines with an increase in the confining stresses, which, in turn, diminishes micro-cracking at different levels. KE was also studied for samples where the confinement pressure was greater than the axial stress. In these models, although KE was less than σ_{1p} , the increased confining pressure did not change the stress caused by models $\sigma_{1p} < \sigma_{3p}$ and the axial stress levels. For example, in the axial pre-stress of 65 MPa, KE in the confining pressure of 80 MPa was greater than the confining pressures of 15, 20, 30, and 50 MPa. Figure 7 shows the estimated stress variation of KE in the confining pre-stress of the models for the axial stresses of 20, 30, 35, 65, 85, and 110 MPa. As shown in the above figure, the changes were similar at all levels of axial stress with an increase in the confining pressure reducing the KE stress. However, the reduction rate of Kaiser Stress was not constant, and it diminished when the confining pre-stress was increased.

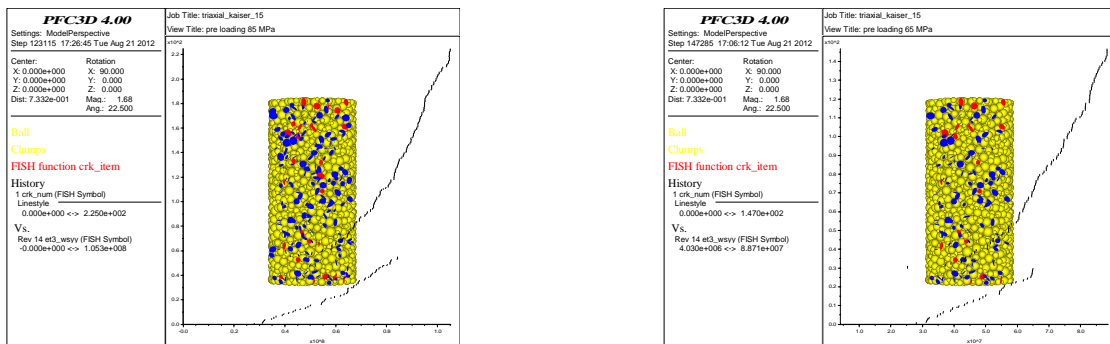


Figure 6. Cumulative total number of recorded cracks versus stress loading in triaxial modeling of cylindrical specimens under axial pre-stresses of 65 MPa (right) and 85 MPa (left) for a confining pressure of 15 MPa (loading path II).

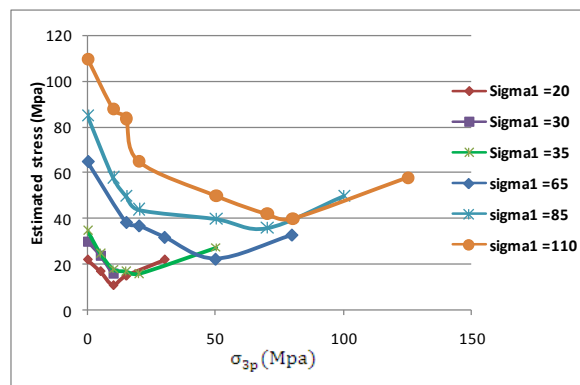


Figure 7. Changes in estimated stress based on confining pre-stresses in axial pre-stresses, modeling of cylindrical specimens (loading path II).

3.4.3. Loading path III

This type of loading path was studied to assess the dependence of the loading triaxial stress and triaxial pre-loading effect on the retrieved stress in the re-loading applied to the axial direction. Initially, similar to loading path II, the first cycle of loading was applied to produce memory with different combinations of stress σ_{3p} and σ_{1p} in accordance with Table 4. The un-loading was performed in the axial direction of the sample to achieve zero stress in the loading planes. Contrary to the loading path II, under this loading path, the next cycle as the reloaded cycle beyond the previous maximum stress under triaxial was applied along with the recording of the cracks in the sample in the axial direction with the confining pressure of σ_{3p} .

The method adopted in accordance with the modeling method was aimed at evaluating the effect of confining pressure under triaxial reloading and determining the KE stress under the triaxial condition. In such a modeling, the pre-loading is used to estimate the pre-loading stress and evaluate the KE point of the number of cumulative cracks as a benchmark for the KE point to estimate the pre-loading stress.

Table 4 shows the results of numerical modeling of this loading path including the KE, damage

coefficient (K), and the ratios $\frac{\sigma_{KE}}{\sigma_{1P}}$ and $\frac{\sigma_{KE}}{\sigma_{1P} - \sigma_{3P}}$

calculated for each model. For example, the accumulation of cracks in the axial stress at the complete pre-loading, un-loading and re-loading cycles of the axial pre-stress of 65 and 85 MPa in a confining pressure of 30 MPa are presented in Figure 8. At this stage, interesting results were derived from the models so that when the confining pressure was relatively low compared to the axial stress, similar results were obtained in the uniaxial tests, and new cracks in the second cycle of loading were not developed before the previously established maximum stress. In other words, KE on the triaxial modeling of reloading was able to retrieve the axial stress values with slight differences in the loading cycle.

As it is evident in Figure 8, the onset point of increasing cracking or KE at stress levels of pre-loading is close to the pre-loading stress levels but despite re-loading to the axial stress level of previous loading, no increase in the cracks was observed. Thus the KE stress is close to the axial stress applied to the sample in the pre-loading cycle. Therefore, it can be concluded that the stress memory of triaxial condition can be retrieved by the triaxial numerical simulation when the confining pressure and the axial pressure difference is large.

Table 4. Results of numerical modeling of cylindrical samples (loading path III).

Sample	Triaxial pre-stress (MPa)		σ_{KE} (Mpa)	K	$\frac{\sigma_{KE}}{\sigma_{1P}}$	$\frac{\sigma_{KE}}{\sigma_{1P} - \sigma_{3P}}$
	σ_{1P}	σ_{3P}				
1	30	5	31	-1.2	-1.03	1.24
2	30	15	32	-1.1	1.06	2.1
3	30	20	32.5	-1.1	1.08	3.25
4	35	5	32.5	-0.5	0.92	1.08
5	35	10		2.5	0	0
6	35	20	40	-1.25	1.1	0.2
7	65	10	65	-1	1	1.1
8	65	15	65	-1	1	1.3
9	65	20	68	-1.1	1.04	1.5
10	65	30	68	-1.1	1.04	1.9
11	65	50	74	-1.18	1.1	4.9
12	85	5	85	-1	1	1.06
13	85	10	85	-1	1	1.1
14	85	15	85	-1	1	1.2
15	85	30	81	-0.8	0.95	1.4
16	85	50	82.5	-0.9	0.9	2.3
17	85	70	85	-1	1	5.6
18	110	10	110	-1	1	1.1
19	110	30	110	-1	1	1.3
20	110	50	110	-1	1	1.8
21	110	70	115	-1.07	1.04	2.8
22	110	80	120	-1.1	1.09	4
23	110	90	125	-1.1	1.1	6.2

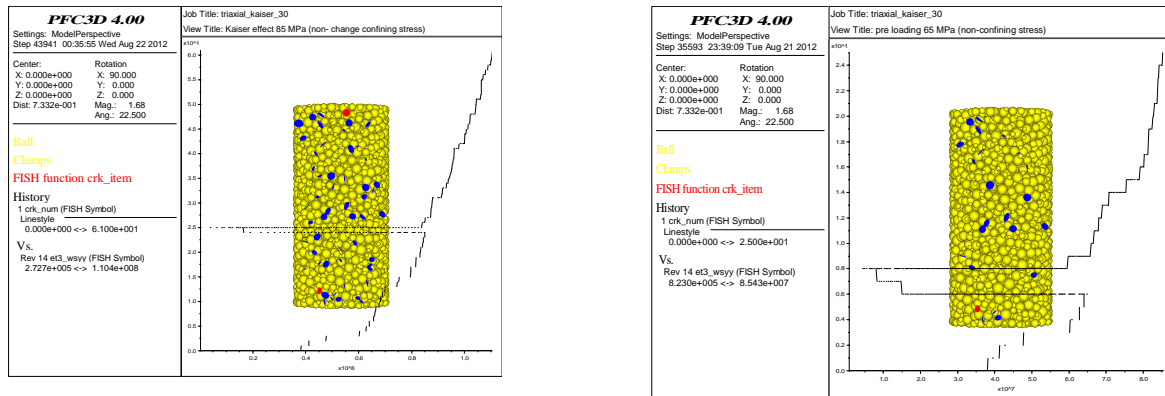


Figure 8. Cumulative total number of recorded cracks versus loading stress in triaxial modeling of cylindrical specimens under axial pre-stresses of 65 MPa (right) and 85 MPa (left) for confining pressure of 30 MPa (loading path III).

As mentioned earlier in loading path II, it is not possible to measure the axial pre-stress in uniaxial condition subjected to triaxial loading. According to Table 4, the stress memory at the axial direction of all stress levels of pre-loading cannot be retrieved so that in samples with a confining pressure to axial pressure ratio of more than 0.3, KE was greater than the axial pre-stress. In this regard, KE of pre-loading rises with an increase in the confining pressure at the same level of axial stress. This can be explained in terms of the effect of confining pressure on the stress required to create cracks in the examples. In other words, if the confining pressure of the pre-loading cycle exceeds a certain axial stress of pre-loading, according to the theory of damage, further stress in the sample will be required to pass the surface damage. For example, KE was 110 MPa for axial pre-loading samples 5, 10, 20, 50, 70, 80 and 90 MPa, for preloading confining pressures, 110 MPa for confining pressure of 5 to 50MPa, and 115, 120, and 124 MPa for confining pressures of 70, 80, and 90 MPa, respectively.

4. Discussion

In the present work, it was shown numerically that, similar to the uniaxial tests performed on physical samples, new cracks did not appear in the second cycle of loading before reaching the previous maximum stress, and that there was no growth in the existing cracks. The simulation results confirmed that the numerical model could produce the Kaiser Effect (KE). It is difficult to provide a full description of the complex nature of KE in real rocks using numerical modeling, which is due to the simplifications and assumptions adopted for the modeling. However, numerical simulations proved a general perception of the nature of KE, according to which, this effect is closely related to the development of cracks with

the triaxial loading and confining stress influencing KE. Despite the difficulty of performing a quantitative comparison of numerical model with physical tests, the qualitative analysis of the impact and effectiveness of the numerical modeling was shown.

KE in the numerical model could be evaluated by monitoring the cumulative number of micro-cracks created in the model. Although the broken bonds representing micro-cracks in the model cannot be directly equated with the value of the AE, the detection and identification of KE is possible through an analysis of curves of the cumulative number of micro-cracks in stresses similar to observations and graphs of AE with respect to the stress or time. Also it should be noted that the AE counts and number of micro-cracks were linked to the crack onset threshold, and by determining a greater threshold stress of the crack onset, a lower number of micro-cracks appeared in the pre-loading. Micro-cracks in the PFC model appear between the sample particles, so their number will be a function of the included particles of model. However, there was no disagreement in the target and pattern obtained, through which KE was examined, and the only difference was the number of micro-cracks. According to the cyclic modeling performed under the uniaxial condition, the stress memory of KE was confirmed, which was observed at different stress levels.

The results of numerical modeling under triaxial of cylindrical specimen indicate the impact of confining pressure on KE and its reductive effect on the retrieval of stress memory. All the numerical studies performed on the effect of confining pressures on the stress of KE revealed that when confining pressure increased in the same axial stress level, the clarity of KE and

detection of the Kaiser Curvature point would be difficult. Also, in this case, greater difference was observed between the axial estimated stress of KE and pre-loading stress in the axial direction. According to the results of the numerical examples in which the first cycle was carried out as the pre-loading of the triaxial case and the re-loading cycle was also performed under the triaxial condition, it can be said that when the confining pressure is relatively lower than the uniaxial stress, similar test results can be obtained. In other words, in these instances, by modeling under triaxial reloading, the stress memory of KE is equal to the axial stress applied or slightly different in the retrieved loading cycle.

5. Conclusions

PFC3d was used to simulate the KE cylindrical specimen under triaxial compression tests. The goal of developing the model was to verify the laboratory testing results of KE observed through a specimen. The influences of confining stress on the aforesaid effect behavior were analyzed. The main conclusions could be described as follow:

- The study revealed that the PFC program and the distinct element numerical method offered a suitable means for analyzing damage to a brittle rock and the KE phenomenon.
- The overall results of the study confirmed that KE could not be verified under uniaxial pressure for the sample subjected to triaxial pressure but if the second cycle was re-loaded under tri-axial stress, the axial pre-stress was retrieved.
- According to the results of the analysis, the amount of stress by the KE could be underestimated so that with an increase in the confining pressure in the rock, a greater difference was observed between the KE stresses obtained from uniaxial loading and the actual stress of the rock.
- The results obtained showed that the estimated stress was not equivalent to the previous vertical stress and the confining stress, except when the confining stress was zero.
- According to the cyclic modeling performed under uniaxial stress, the stress memory of KE was confirmed, and this effect was observed at different levels of stress.
- The combination of triaxial loading stress in samples change the results, and the studies show that KE is placed under triaxial loading and confining stresses.

- According to the results of the study, uniaxial loading of a rock sample was unable to show a triaxial stress history because the onset stress of AE was a function of the three principal stresses applied to the rock mass.

References

- [1]. Tensi, H.M. (2004). The Kaiser-effect and its scientific background. Paper presented at the 26th European conference on acoustic emission testing.
- [2]. Lavrov, A. (2003). The Kaiser effect in rocks: principles and stress estimation techniques. *International Journal of Rock Mechanics and Mining Sciences*. 40 (2): 151-171.
- [3]. Tang, C. and Kou, S. (1998). Crack propagation and coalescence in brittle materials under compression. *Engineering Fracture Mechanics*. 61 (3): 311-324.
- [4]. Chen, Z., Tham, L. and Xie, H. (2007). Experimental and numerical study of the directional dependency of the Kaiser effect in granite. *International Journal of Rock Mechanics and Mining Sciences*. 44 (7): 1053-1061.
- [5]. Lavrov, A., Vervoort, A. and Napier, J. (2002). Experimental and numerical studies of damage development in rock under cyclic loading. Paper presented at the 2nd International Biot conference on poromechanics.
- [6]. Lavrov, A., Vervoort, A., Wevers, M. and Napier, J. (2002). Experimental and numerical study of the Kaiser effect in cyclic Brazilian tests with disk rotation. *International Journal of Rock Mechanics and Mining Sciences*. 39 (3): 287-302.
- [7]. Hunt, S., Meyers, A. and Louchnikov, V. (2003). Modelling the Kaiser effect and deformation rate analysis in sandstone using the discrete element method. *Computers and Geotechnics*. 30 (7): 611-621.
- [8]. Holt, R., Kjølås, J., Larsen, I., Li, L., Pillitteri, A.G. and Sønstebø, E. (2005). Comparison between controlled laboratory experiments and discrete particle simulations of the mechanical behaviour of rock. *International Journal of Rock Mechanics and Mining Sciences*. 42 (7): 985-995.
- [9]. Gorodkov, S., Li, L. and Holt, R. (2006). Stress path during coring: a discrete particle modeling approach. In- *Situ Rock Stress*. Taylor & Francis Group. pp. 541-549.
- [10]. Itasca, C. (2009). PFC 3d-user manual. Itasca Consulting Group. Minneapolis.
- [11]. Potyondy, D. and Cundall, P. (2004). A bonded-particle model for rock. *International Journal of Rock Mechanics and Mining Sciences*. 41 (8): 1329-1364.
- [12]. Lisjak, A. and Grasselli, G. (2014). A review of discrete modeling techniques for fracturing processes

in discontinuous rock masses. *Journal of Rock Mechanics and Geotechnical Engineering*. 6: 301-314

[13]. Kaiser, P., Diederichs, M., Martin, C., Sharp, J. and Steiner, W. (2000). Underground works in hard rock tunnelling and mining. Paper presented at the ISRM International Symposium.

[14]. Zhang, X.P. and Wong, L.N.Y. (2012). Cracking processes in rock-like material containing a single flaw under uniaxial compression: a numerical study based on bonded-particle model approach. *Rock Mechanics and Rock Engineering*. 45 (5): 711-737.

[15]. Zhang, X.P. and Wong, L.N.Y. (2013). Crack initiation, propagation and coalescence in rock-like material containing two flaws: a numerical study based on bonded-particle model approach. *Rock Mechanics and Rock Engineering*. 46 (5): 1001-1021.

[16]. Chang, S.H., Yun, K.J. and Lee, C.I. (2002). Modeling of fracture and damage in rock by the bonded-particle model. *Geosystem Engineering*. 5 (4): 113-120.

[17]. Chang, S.H. and Lee, C.I. (2004). Estimation of cracking and damage mechanisms in rock under triaxial compression by moment tensor analysis of acoustic emission. *International Journal of Rock Mechanics and Mining Sciences*. 41 (7): 1069-1086.

[18]. Chang, S.H., Lee, C.I. and Lee, Y.K. (2007). An experimental damage model and its application to the evaluation of the excavation damage zone. *Rock mechanics and rock engineering*. 40 (3): 245-285.

[19]. Holt, R., Doornhof, D. and Kenter, C. (2002). Use of discrete particle modeling to understand

stress-release effects on mechanical and petrophysical behavior of granular rocks. Paper presented at the Numerical Modeling in Micromechanics via Particle Methods (Proceedings of the 1st International PFC Symposium). Gelsenkirchen. Germany.

[20]. Mitra, R. and Westman, E. (2009). Investigation of the stress imaging in rock samples using numerical modeling and laboratory tomography. *International Journal of Geotechnical Engineering*. 3 (4): 517-525.

[21]. Wanne, T. and Young, R. (2008). Bonded-particle modeling of thermally fractured granite. *International Journal of Rock Mechanics and Mining Sciences*. 45 (5): 789-799.

[22]. Yoon, J.S., Zang, A. and Stephansson, O. (2012). Simulating fracture and friction of Aue granite under confined asymmetric compressive test using clumped particle model. *International Journal of Rock Mechanics and Mining Sciences*. 49: 68-83.

[23]. Cho, N.A., Martin, C. and Sego, D. (2007). A clumped particle model for rock. *International Journal of Rock Mechanics and Mining Sciences*. 44 (7): 997-1010.

[24]. Scholtes, L. and Donze, F.V. (2013). A DEM model for soft and hard rocks: Role of grain interlocking on strength. *Journal of the Mechanics and Physics of Solids*. 61: 352-369.

[25]. Ghazvinian, E. and Diederichs, M. (2010). A comparison between application of two and three dimensional bonded-particle models for simulation of damage accumulation in rock. *Rock Mechanics in Civil and Environmental Engineering*. pp. 181-184.

ارزیابی عددی تأثیر تنش جانبی بر روی اثر کایزر با استفاده از روش المان مجزا

مجید نیکخواه

دانشکده مهندسی معدن، نفت و ژئوفیزیک، دانشگاه صنعتی شاهرود، ایران

ارسال ۲۰۱۵/۱۲/۱۱، پذیرش ۲۰۱۶/۹/۹

نویسنده مسئول مکاتبات: m.nikkhah@shahroodut.ac.ir

چکیده:

امروزه استفاده از آزمایش انتشار اکوستیک مبتنی بر اثر کایزر به منظور تخمین تنش برجا در آزمایشگاه بر روی مغزه‌های حفاری رو به فزونی است. در این تحقیق، اثر کایزر بر اساس شبیه‌سازی‌های عددی بارگذاری سیکلی مشتمل بر بارگذاری- باربرداری و بارگذاری مجدد، با استفاده از نرم‌افزار سه‌بعدی المان مجزا PFC بر روی نمونه‌های پیش بارگذاری شده تحت حالت تنش سه محوره و تک محوره بر روی نمونه‌های استوانه‌ای ارزیابی شده است. در راستای نیل به اهداف مذکور، ابتدا مدل عددی با استفاده از نتایج آزمون‌های آزمایشگاهی انجام شده بر روی نمونه انتخابی ماسه‌سنگ واسنجی شده است. بر اساس مدل‌سازی‌های سیکلی انجام شده در شرایط تک محوره، وجود حافظه تنش اثر کایزر تأیید شده و این اثر در سطوح مختلف تنش مشاهده شد. نتایج نشان می‌دهند که ترکیبات تنش بارگذاری سه محوره مختلف در نمونه‌ها، باعث تغییر در نتایج بارگذاری تک محوری گردیده و اثر کایزر تحت تأثیر تنش‌های جانبی و بارگذاری سه محوره قرار می‌گیرد، به طوری که تنش جانبی بزرگ‌تر منجر به اختلاف بیشتری بین تنش اثر کایزر به دست آمده از بارگذاری تک محوره و پیش تنش محوری می‌شود.

کلمات کلیدی: اثر کایزر، تنش جانبی، مدل‌سازی عددی، سنگ، PFC.
